JACS
JOURNAL OF THE AMERICAN CHEMICAL SOCIETY
pubs.acs.org/JACS
Article

Three-Dimensional Covalent Organic Frameworks with Ultra-Large Pores for Highly Efficient Photocatalysis

Jiehua Ding,[‖] Xinyu Guan,[‖] Jia Lv, Xiaohong Chen, Yi Zhang, Hui Li, Daliang Zhang, Shilun Qiu, Hai-Long Jiang,* and Qianrong Fang*

Cite This: J. Am. Chem. Soc. 2023, 145, 3248−3254

ABSTRACT: Benefiting from their unique structural merits, three-dimensional (3D) large-pore COF materials demonstrate high surface areas and interconnected large channels, which makes these materials promising in practical applications. Unfortunately, functionalization strategies and application research are still absent in these structures. To this end, a series of functional 3D **stp**-topologized COFs are designed based on porphyrin or metalloporphyrin moieties, named JUC-640-M (M = Co, Ni, or H). Interestingly, JUC-640-H exhibits a record-breaking low crystal density (0.106 $cm^3\ g^{-1}$) among all crystalline materials, along with the largest interconnected pore size (4.6 nm) in 3D COFs, high surface area (2204 $m^2\ g^{-1}$), and abundant exposed porphyrin moieties (0.845 mmol g^{-1}). Inspired by the unique structural characteristics and photoelectrical performance, JUC-640-Co is utilized for the photoreduction of CO_2 to CO and demonstrates a high CO production rate (15.1 mmol $g^{-1}\ h^{-1}$), selectivity (94.4%), and stability. It should be noted that the CO production rate of JUC-640-Co has exceeded those of all reported COF-based materials. This work not only produces a series of novel 3D COFs with large channels but also provides a new guidance for the functionalization and applications of COFs.

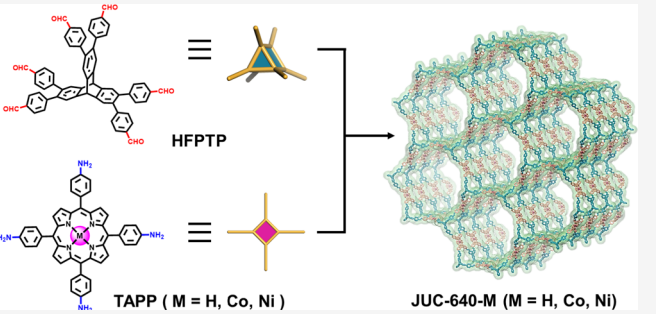

INTRODUCTION

Covalent organic frameworks (COFs), extensively studied members of crystalline porous materials (CPMs), are assembled with strong covalent bonds and distinguish themselves from amorphous porous polymers in their topological designability, structural tunability, and functional predictability.[1,2] These materials are potential candidates for applications in gas adsorption,[3−6] molecular separation,[7−11] molecular recognition,[12−16] energy storage,[17−20] heterogeneous catalysis,[21−29] etc. Different from two-dimensional (2D) counterparts in which layered networks are connected via intraplane covalent bonding and further stacked via weak interactions, three-dimensional (3D) COFs possess isolated building blocks to construct nonplanar periodic networks with unique structures and properties.[30,31]

To date, most reported functional 3D COFs are based on tetrahedral (T_d) building blocks with topologies such as **dia**[32,33] and **pts**,[34−36] which restrict the structural diversity and functional regulation of 3D COFs. More importantly, interpenetration as a common phenomenon in these T_d-based structures will result in the significantly decreased surface area and shrunk pore sizes, which are disadvantageous for various applications, such as adsorption and heterogeneous catalysis. As a result, non-interpenetrated structures with large channels and high surface areas are highly demanded. In previous studies, we reported the first **stp**-topologized 3D COF, named JUC-564, on the basis of the triptycene-based block (D_{3h} symmetrized).[37] Interestingly, the noninterpenetrated framework exhibits a high surface area (3383 $m^2\ g^{-1}$), ultra-large pore size (up to 4.3 nm), and low density (0.108 $cm^3\ g^{-1}$). These fascinating merits endow **stp**-based frameworks with potential in ample application fields. However, no functionalization has been realized in such COFs and applications have never been investigated up to now.

Porphyrin and its metallized derivatives, typical 18 e^- π-conjugated macrocycles,[38] have been widely employed as organic catalytic centers and implanted on crystalline porous supports such as metal−organic frameworks (MOFs) and COFs.[39−42] Porphyrin-based frameworks have been widely explored as heterogeneous catalysts, such as photocatalytic carbon dioxide (CO_2) reduction,[43−46] a particularly promising strategy to reduce the abundant emission of CO_2 and transform solar energy into chemicals or fuels.

Received: December 28, 2022
Published: January 31, 2023

https://doi.org/10.1021/jacs.2c13817
J. Am. Chem. Soc. 2023, 145, 3248−3254

Scheme 1. Molecular Structures of (a) HFPTP as a Six-Connected 3D-D_{3h} Core Building Block, (b) TAPP-M as a Synergistic Four-Connected 2D-D_{4h} Monomer, (c) Structures of Novel 3D COFs, JUC-640-M (M = H, Co, or Ni), Constructed from the Condensation Reaction of HFPTP and TAPP-M, and Expanded Framework for (d) JUC-640-M and e) stp Net

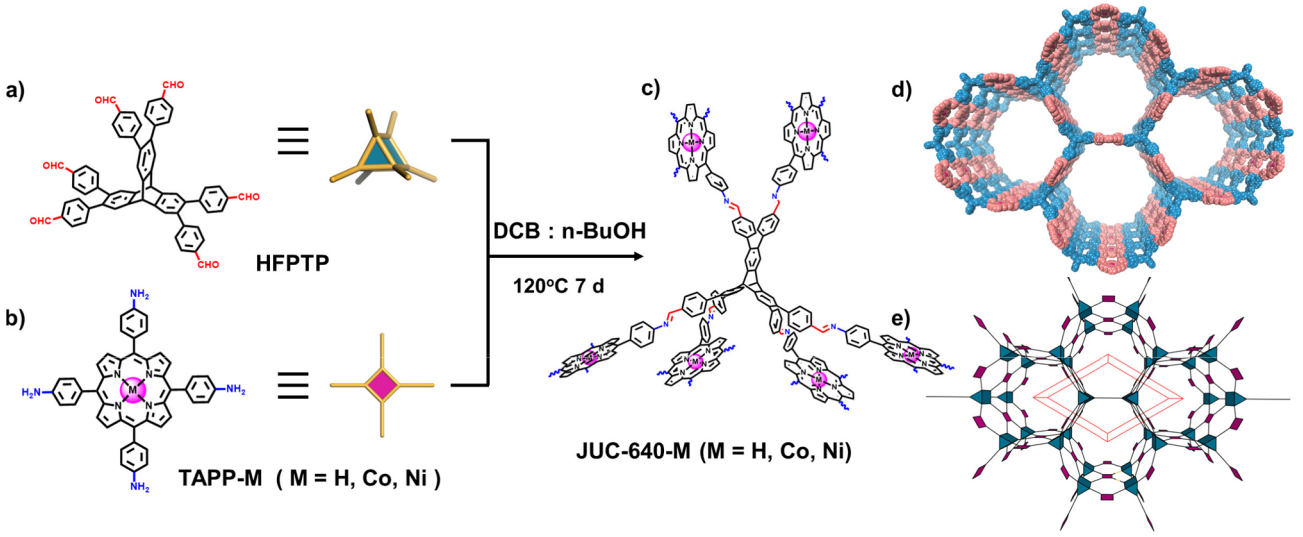

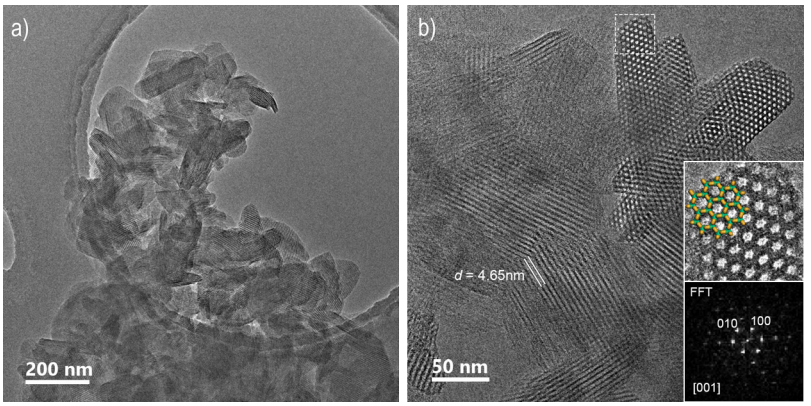

Figure 1. (a) TEM image and (b) high-resolution TEM image of JUC-640-H. Marked area in (b) has been cropped and scaled up in the inset with the structure model overlaid. The FFT of the cropped area has been indexed as the [001] zone axis.

Herein, inspired by the structural advantages of **stp**-topologized frameworks and the unique photoelectric properties of porphyrin moieties, a serial of novel 3D porphyrin COFs (JUC-640-M, M = H, Co, or Ni) are designed and prepared based on the **stp** net. It should be noted that the extremely low crystal density (0.106 $cm^3\ g^{-1}$) of JUC-640-H is a new record among all crystalline materials, and the interconnected channels (up to 4.6 nm) are also the largest in 3D COFs. Benefiting from the high surface area (2204 $m^2\ g^{-1}$), large interpenetrated channels, and abundant exposed porphyrin moieties (0.845 mmol g^{-1}), these crystalline materials are explored as photocatalysts for CO_2 reduction under visible light irradiation with record high activity (15.1 mmol $g^{-1}\ h^{-1}$), along with good selectivity (94.4%) and stability (at least 5 cycles).

RESULTS AND DISCUSSION

Typically, JUC-640-M was crystallized under traditional solvothermal conditions by polymerizing the 6-connected triptycene-based building unit, 2,3,6,7,14,15-hexa(4′-formylphenyl)triptycene (HFPTP, D_{3h}-symmetrized), with the 4-connected 5,10,15,20-tetrakis(4-aminophenyl)porphyrin (TAPP-H, D_{4h}-symmetrized) or its metallized derivatives (TAPP-Co and TAPP-Ni) (Scheme 1). Complementary characterization techniques were employed for structural definition. The formation of imine linkages could be confirmed by the new peaks (approximately 1622 cm^{-1}) in the Fourier transform infrared (FTIR) spectra (Supporting Information, Figures S13−S15). The successful transformation could further be confirmed by the disappearance of C═O vibrations (approximately 1699 cm^{-1}) and N−H vibrations (approximately 3350 cm^{-1}) in the FTIR spectra. Solid-state ^{13}C cross-polarization/magic-angle-spinning (CP/MAS) NMR spectroscopy further verified the presence of imine groups by the peak at ∼159 ppm (Supporting Information, Figures S16−S18). Scanning electron microscopy (SEM) and transmission electron microscopy (TEM) exhibited the morphology of JUC-640-M as microcrystal aggregates. No clear nanoparticles could be observed for JUC-640-Co and JUC-640-Ni in TEM images, suggesting that the metal exists as isolated sites (Figure 1a and Supporting Information, Figures S6−S10). Subsequently, the microcrystals of JUC-640-Co and JUC-640-Ni were further analyzed by energy-dispersive X-ray (EDX) mapping, which demonstrates that metalloporphyrin sites are uniformly dispersed in the skeletons (Supporting Information,

https://doi.org/10.1021/jacs.2c13817
J. Am. Chem. Soc. 2023, 145, 3248−3254

Figures S11 and S12). The metal contents were determined to be 4.87% JUC-640-Co and 4.36% for JUC-640-Ni based on inductively couple plasma-optical emission spectrometry (ICP-OES), which is basic anastomotic with the results predicted from the crystal structures. The corresponding electronic states of Co and Ni species were further investigated by X-ray photoelectron spectroscopy (XPS) (Figure 4c and Supporting Information, Figures S31−S34). Notably, the binding energies sited about 780.0 and 795.2 eV in JUC-640-Co and 854.6 and 871.7 eV in JUC-640-Ni, which can be identified as +2 oxide states in the Co 2p spectra and Ni 2p spectra, respectively. Thermogravimetric analysis (TGA) illustrated good thermal stability (about 400 °C) of JUC-640-M under a nitrogen atmosphere (Supporting Information, Figures S19−S21).

The crystalline structures of JUC-640-M were identified by powder X-ray diffraction (PXRD) in conjugation with structural simulation on the basis of the material studio software package[47] (Supporting Information, Tables S2−S4). After the geometrical energy minimization based on the **stp** network, unit cell parameters were acquired ($a = b = 54.6648$ Å, $c = 20.6969$ Å, $\alpha = \beta = 90°$, and $\gamma = 120°$ for JUC-640-H; $a = b = 54.6266$ Å, $c = 21.5251$ Å, $\alpha = \beta = 90°$, and $\gamma = 120°$ for JUC-640-Co; $a = b = 54.5707$ Å, $c = 21.5094$ Å, $\alpha = \beta = 90°$, and $\gamma = 120°$ for JUC-640-Ni), which provided well compatible predicted PXRD patterns with the experimental ones (Figure 2a,c,e). Subsequently, full profile pattern matching (Pawley) refinements were carried out and exhibited low agreement factors ($R_p = 1.49\%$ and $R_{wp} = 1.76\%$ for JUC-640-H; $R_p = 1.58\%$ and $R_{wp} = 2.29\%$ for JUC-640-Co; $R_p = 1.64\%$ and $R_{wp} = 1.99\%$ for JUC-640-Ni). Hexagonal-arranged channels could be clearly seen from high-resolution TEM images (Figure 1b). The measured *d*-spacing of 100 and 010 reflections was 4.65 nm that presented a good match of the proposed structure model. As a result, JUC-640-M were demonstrated to be 3D frameworks based on the non-interpenetrated **stp** net. Notably, JUC-640-H exhibited an extremely low crystal density (0.106 $cm^3\ g^{-1}$), which breaks the record in COF materials. Moreover, these materials exhibited the largest interpenetrated channels (up to 4.6 nm) among all 3D COFs as well as densely populated porphyrin sites (0.845 mmol g^{-1}), making JUC-640-M a perfect platform for heterogeneous catalysis. Nitrogen adsorption−desorption isotherms were carried out under 77 K to investigate the pore structures of these crystalline frameworks. As shown in Figure 2b,d,f, all JUC-640-M exhibited typical type IV isotherms, which revealed the mesoporous characteristics. The specific surface areas were calculated up to be 2204 $m^2\ g^{-1}$ according to the Brunauer−Emmett−Teller (BET) equation (Supporting Information, Figures S35−S37). On the basis of nonlocal density functional theory (NLDFT) calculations, JUC-640-M exhibited the pore size distribution with mesopores up to 4.3 nm, in accordance with the results predicted from the modeled crystal structures (4.6 nm) shown in Figure 3, which further

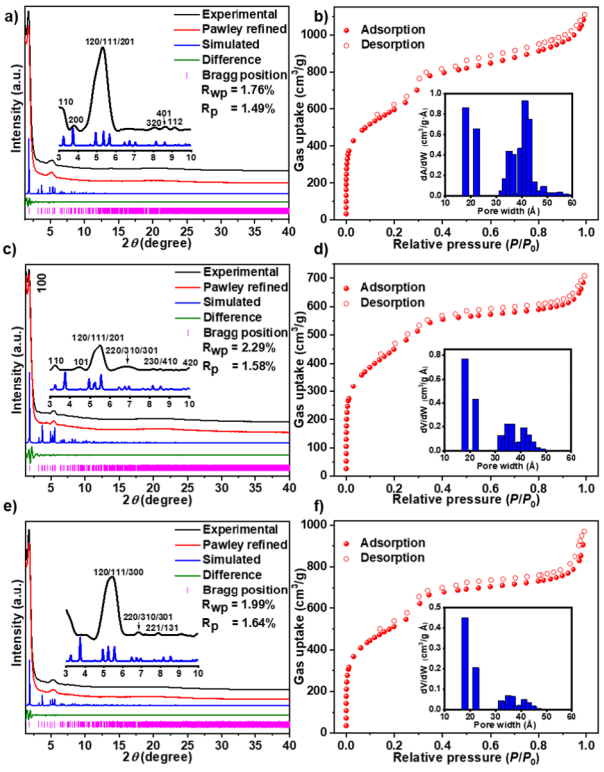

Figure 2. Experimental and refined PXRD patterns of (a) JUC-640-H, (c) JUC-640-Co, and (e) JUC-640-Ni. N_2 adsorption−desorption isotherms of (b) JUC-640-H, (d) JUC-640-Co, and (f) JUC-640-Ni at 77 K (inset: pore-size distribution profiles).

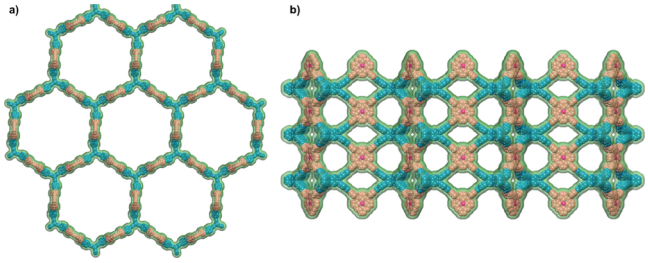

Figure 3. Extended structure of JUC-640-M viewed along (a) the *c* axis and (b) the *a* or *b* axis. Triptycene, green; porphyrin, burlywood; M, magenta.

confirms the noninterpenetrated structure of JUC-640-M. Subsequently, to investigate the CO_2 affinity, the CO_2 adsorption behaviors of these COFs were measured under 1 bar. All three **stp**-based COFs exhibited moderate CO_2 capacity, which are 52.16 $cm^3\ g^{-1}$ at 273 K and 31.88 $cm^3\ g^{-1}$ at 298 K for JUC-640-H, 65.78 $cm^3\ g^{-1}$ at 273 K and 41.18 $cm^3\ g^{-1}$ at 298 K for JUC-640-Ni, and 57.43 $cm^3\ g^{-1}$ at 273 K and 37.83 $cm^3\ g^{-1}$ at 298 K for JUC-640-Co, suggesting their potential in CO_2 uptake and conversion (Supporting Information, Figures S38−S40). Meanwhile, based on CO_2 adsorption isotherms at 273 and 298 K, the isosteric heats of adsorption (Q_{st}) for CO_2 were calculated to be 20.6 kJ mol^{-1} for JUC-640-Co, 16.2 kJ mol^{-1} for JUC-640-Ni, and 10.2 kJ mol^{-1} for JUC-640-H, implying the superior CO_2 affinity for JUC-640-Co compared with JUC-640-Ni and JUC-640-H (Supporting Information, Figures S41−S43).

Subsequently, photoelectrical measurements were carried out for these COFs. Solid-state UV−vis diffuse reflectance spectroscopy (DRS) showed their strong light-harvesting ability in the UV and visible light regions (Supporting Information, Figures S22, S24 and S26). Based on the Kubelka-Munk (KM) method, their band gap energies (E_g) were acquired via the Tauc plots to be 1.98 eV for JUC-640-Co, 1.84 eV for JUC-640-Ni, and 1.77 eV for JUC-640-H, respectively (Figure 4a and Supporting Information, Figures S23, S25, and S27). Subsequently, Mott-Schottky measure-

https://doi.org/10.1021/jacs.2c13817
J. Am. Chem. Soc. 2023, 145, 3248−3254

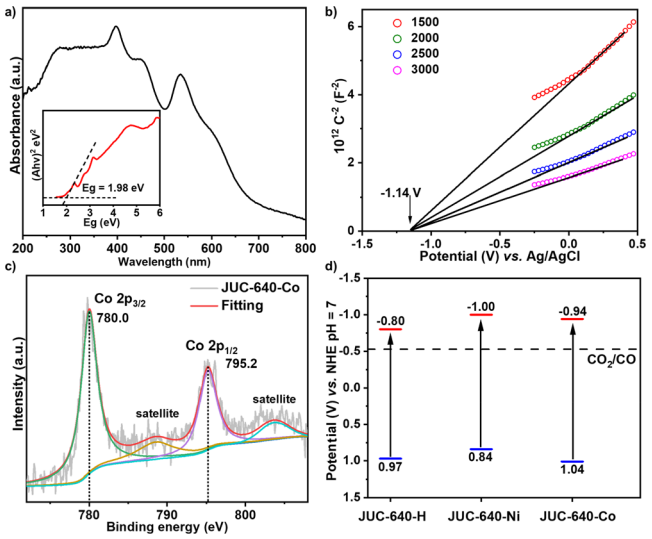

Figure 4. (a) UV−vis spectra and Tauc plot (inset), (b) Mott−Schottky plots, (c) XPS Co 2p spectra of JUC-640-Co, and (d) band structure diagram for JUC-640-M.

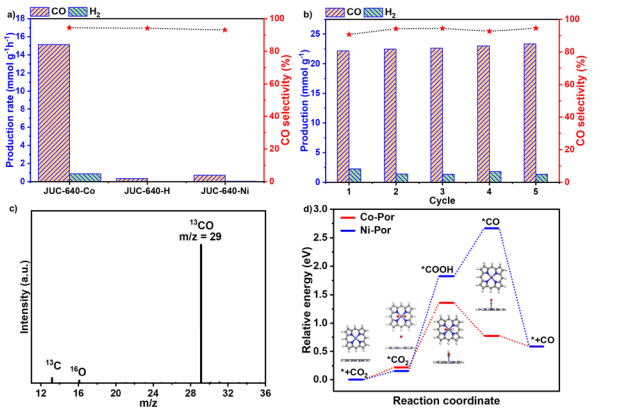

Figure 5. (a) Comparison of the photocatalytic activity of JUC-640-M, conditions: 3 mg of COF, 5 mg of $Ru(bpy)_3Cl_2·6H_2O$, 50 mg of BIH, 8 mL of MeCN, 12 mL of water, 300 W Xe lamp (≥ 380 nm), 1 h, (b) durability measurements of JUC-640-Co (2 h each cycle), (c) ^{13}C isotopic experiment for JUC-640-Co, and (d) free energy diagrams for CO_2 reduction to CO on JUC-640-M (M = Co or Ni).

ments were performed to determine the band positions (Figure 4b and Supporting Information, Figures S28 and S29). According to the intersections with the *x*-axis, the flat bands (equal to lowest unoccupied molecular orbitals, LUMO) are determined as −0.94, −1.00, and −0.80 V vs normal hydrogen electrode (NHE) corresponding to JUC-640-Co, JUC-640-Ni, and JUC-640-H. In conjugation with the band gaps obtained from UV−vis DRS, the highest occupied molecular orbitals (HOMO) were calculated to be 1.04, 0.84, and 0.97 V vs NHE for JUC-640-Co, JUC-640-Ni, and JUC-640-H, respectively (Figure 4d). Significantly, all the LUMO potentials were more negative compared with those of H_2O/H_2 (0 V vs NHE) and CO_2/CO (0.51 V vs NHE), implying their essential feasibility for photocatalytic H_2 evolution and CO_2 reduction. In the electrochemical impedance spectroscopy (EIS), JUC-640-Co showed a smaller semicircle radius of the Nyquist plot than those of JUC-640-Ni and JUC-640-H, which implied a more rapid interfacial charge transfer in JUC-640-Co (Supporting Information, Figure S30).

Encouraged by the interpenetrated porous structures, abundant exposed porphyrin sites, and fascinating photoelectrical performance, JUC-640-M was employed for the photoreduction of CO_2. The photocatalytic experiments were performed under visible light irradiation ($\lambda \geq 380$ nm) in the mixed solution of acetonitrile and water (v/v = 2/3) using 1,3-dimethyl-2-phenyl-2,3-dihydro-1*H*-benzo[*d*]imidazole (BIH) as the sacrificial agent and $Ru(bpy)_3Cl_2·6H_2O$ as the photosensitizer (Supporting Information, Figure S47). CO and H_2 were identified as the major photoreduction products with negligible other gaseous or liquid products (e.g., CH_4, CH_3OH, and HCOOH) (Supporting Information, Figure S48). Encouragingly, JUC-640-Co exhibited an extremely high CO production rate (15.1 mmol g^{-1} h^{-1}) as well as high selectivity (94.4%, Figure 5a). It should be noted that the CO production rate of JUC-640-Co is a new record in all reported COF-based materials (Supporting Information, Table S1). Moreover, the apparent quantum efficiency (AQE) of JUC-640-Co was measured at different wavelengths, which reached up to 1.48% at 450 nm (Supporting Information, Figure S49). As a comparison, JUC-640-Ni and JUC-640-H demonstrate lower CO production rates under similar conditions due to the different active sites. Almost no reduction products could be observed without the existence of irradiation, CO_2, or COFs (Supporting Information, Figure S50). Moreover, JUC-640-Co exhibits high photocatalytic stability, which was evidenced by the negligibly changed CO production rates and selectivity after at least 5 cycles (Figure 5b and Supporting Information, Figures S44 and S45). To further determine the carbon origin of photocatalysis products, an isotopic experiment was performed under similar photocatalytic conditions but using $^{13}CO_2$ as the carbon source (Figure 5c). As a result, the production of ^{13}CO (m/z = 29) could be significantly identified via gas chromatography−mass spectrometry (GC−MS), suggesting that the generated CO came from CO_2.

To better understand the mechanism of CO_2 photoreduction on the metalloporphyrin-derived frameworks, density functional theory (DFT) calculations were carried out with metalloporphyrin fragments as the models (Supporting Information, Figure S46). Gibbs free-energy diagrams of CO_2 reduction on cobalt−porphyrin (Co-Por) and nickel−porphyrin (Ni-Por) are presented in Figure 5d. In the four-step procedures for the photoreduction of CO_2, including CO_2 adsorption, COOH* formation, CO* generation, and CO desorption, the formations of COOH* ($CO_2^* + H^+ + e^- \rightarrow$ COOH*) were determined as the rate-determining step in both Co-Por and Ni-Por, with the highest free-energy barriers (1.23 eV for Co-Por and 1.67 eV for Ni-Por). As a result, the better CO_2 reduction performance on JUC-640-Co could be put down to the significantly lower free-energy barrier of Co-Por, compared with its nickelic counterparts, which were well compatible with the previously reported metalloporphyrin-based frameworks.[48]

CONCLUSIONS

In conclusion, a series of 3D COFs (JUC-640-M) were designed and synthesized based on **stp** topology and porphyrin functionalization. Remarkably, the metal-free JUC-640-H showed a record-breaking low crystal density (0.106 cm^3 g^{-1}) among all crystalline materials reported so far, along with the largest pore size (4.6 nm) in 3D COFs, high surface area (2204 m^2/g), and abundant exposed porphyrin moieties

https://doi.org/10.1021/jacs.2c13817
J. Am. Chem. Soc. 2023, 145, 3248−3254

(0.845 mmol g^{-1}), which made JUC-640-M a potential platform for various applications. Encouraged by the distinct photoelectrical performance of metalloporphyrin, JUC-640-M was employed for the photocatalytic reduction of CO_2. Fascinatingly, JUC-640-Co exhibited high CO production rates (15.1 mmol g^{-1} h^{-1}) as well as selectivity (94.4%), exceeding all reported COF-based catalysts. Therefore, this work broadens in favor of the diversities of COF structures and indicates that functional COF materials would be promising candidates for CO_2 reduction catalysts.

■ ASSOCIATED CONTENT

Supporting Information

The Supporting Information is available free of charge at https://pubs.acs.org/doi/10.1021/jacs.2c13817.

Methods and synthetic procedures; NMR spectra; PXRD, SEM, TEM, EDS, FTIR, TGA, BET plot, and UV−vis DRS patterns; Mott−Schottky plots; EIS plots; gas adsorption; stability test; DFT theoretical calculation; catalytic performance; and unit cell parameters (PDF)

■ AUTHOR INFORMATION

Corresponding Authors

Hai-Long Jiang − *Department of Chemistry, University of Science and Technology of China, Hefei, Anhui 230026, P. R. China;* orcid.org/0000-0002-2975-7977; Email: jianglab@ustc.edu.cn

Qianrong Fang − *State Key Laboratory of Inorganic Synthesis and Preparative Chemistry, Jilin University, Changchun 130012, P. R. China;* orcid.org/0000-0003-3365-5508; Email: qrfang@jlu.edu.cn

Authors

Jiehua Ding − *State Key Laboratory of Inorganic Synthesis and Preparative Chemistry, Jilin University, Changchun 130012, P. R. China*

Xinyu Guan − *Department of Chemistry, University of Science and Technology of China, Hefei, Anhui 230026, P. R. China*

Jia Lv − *Multi-Scale Porous Materials Center, Institute of Advanced Interdisciplinary Studies & School of Chemistry and Chemical Engineering, Chongqing University, Chongqing 400044, P. R. China*

Xiaohong Chen − *State Key Laboratory of Inorganic Synthesis and Preparative Chemistry, Jilin University, Changchun 130012, P. R. China*

Yi Zhang − *Department of Chemistry, University of Science and Technology of China, Hefei, Anhui 230026, P. R. China*

Hui Li − *State Key Laboratory of Inorganic Synthesis and Preparative Chemistry, Jilin University, Changchun 130012, P. R. China*

Daliang Zhang − *Multi-Scale Porous Materials Center, Institute of Advanced Interdisciplinary Studies & School of Chemistry and Chemical Engineering, Chongqing University, Chongqing 400044, P. R. China*

Shilun Qiu − *State Key Laboratory of Inorganic Synthesis and Preparative Chemistry, Jilin University, Changchun 130012, P. R. China*

Complete contact information is available at: https://pubs.acs.org/10.1021/jacs.2c13817

Author Contributions

‖J.D. and X.G. contributed equally to this work.

Notes

The authors declare no competing financial interest.

■ ACKNOWLEDGMENTS

This work was supported by the National Key Research and Development Program of China (2021YFA1500400, 2022YFB3704900, and 2021YFF0500500), the National Natural Science Foundation of China (21725101, 22205224, 22025504, 21621001, 21390394, and 22105082), "111" project (BP0719036 and B17020), China Postdoctoral Science Foundation (BX2021281, 2021M703064, 2020TQ0118, and 2020M681034), Fundamental Research Funds for the Central Universities (WK2060000041), and the program for JLU Science and Technology Innovative Research Team.

■ REFERENCES

(1) Diercks, C. S.; Yaghi, O. M. The Atom, the Molecule, and the Covalent Organic Framework. *Science* **2017**, *355*, No. eaal1585.

(2) Liu, R.; Tan, K. T.; Gong, Y.; Chen, Y.; Li, Z.; Xie, S.; He, T.; Lu, Z.; Yang, H.; Jiang, D. Covalent Organic Frameworks: An Ideal Platform for Designing Ordered Materials and Advanced Applications. *Chem. Soc. Rev.* **2021**, *50*, 120−242.

(3) Yu, C.; Li, H.; Wang, Y.; Suo, J.; Guan, X.; Wang, R.; Valtchev, V.; Yan, Y.; Qiu, S.; Fang, Q. Three-Dimensional Triptycene-Functionalized Covalent Organic Frameworks with Hea Net for Hydrogen Adsorption. *Angew. Chem., Int. Ed.* **2022**, *61*, No. e202117101.

(4) Li, Z.; Feng, X.; Zou, Y.; Zhang, Y.; Xia, H.; Liu, X.; Mu, Y. A 2D Azine-Linked Covalent Organic Framework for Gas Storage Applications. *Chem. Commun.* **2014**, *50*, 13825−13828.

(5) Han, S. S.; Furukawa, H.; Yaghi, O. M.; Goddard, W. A. Covalent Organic Frameworks as Exceptional Hydrogen Storage Materials. *J. Am. Chem. Soc.* **2008**, *130*, 11580−11581.

(6) Ma, Y. X.; Li, Z. J.; Wei, L.; Ding, S. Y.; Zhang, Y. B.; Wang, W. A Dynamic Three-Dimensional Covalent Organic Framework. *J. Am. Chem. Soc.* **2017**, *139*, 4995−4998.

(7) Huang, J.; Han, X.; Yang, S.; Cao, Y.; Yuan, C.; Liu, Y.; Wang, J.; Cui, Y. Microporous 3D Covalent Organic Frameworks for Liquid Chromatographic Separation of Xylene Isomers and Ethylbenzene. *J. Am. Chem. Soc.* **2019**, *141*, 8996−9003.

(8) Han, X.; Huang, J.; Yuan, C.; Liu, Y.; Cui, Y. Chiral 3D Covalent Organic Frameworks for High Performance Liquid Chromatographic Enantioseparation. *J. Am. Chem. Soc.* **2018**, *140*, 892−895.

(9) Liu, Y.; Li, W.; Yuan, C.; Jia, L.; Liu, Y.; Huang, A.; Cui, Y. Two-Dimensional Fluorinated Covalent Organic Frameworks with Tunable Hydrophobicity for Ultrafast Oil-Water Separation. *Angew. Chem., Int. Ed.* **2022**, *134*, No. e202113348.

(10) Ma, H.; Ren, H.; Meng, S.; Yan, Z.; Zhao, H.; Sun, F.; Zhu, G. A 3D Microporous Covalent Organic Framework with Exceedingly High C_3H_8/CH_4 and C_2 Hydrocarbon/CH_4 Selectivity. *Chem. Commun.* **2013**, *49*, 9773−9775.

(11) Natraj, A.; Ji, W.; Xin, J.; Castano, I.; Burke, D. W.; Evans, A. M.; Strauss, M. J.; Ateia, M.; Hamachi, L. S.; Gianneschi, N. C.; Alothman, Z. A.; Sun, J.; Yusuf, K.; Dichtel, W. R. Single-Crystalline Imine-Linked Two-Dimensional Covalent Organic Frameworks Separate Benzene and Cyclohexane Efficiently. *J. Am. Chem. Soc.* **2022**, *144*, 19813−19824.

(12) Liu, Y.; Ren, J.; Wang, Y.; Zhu, X.; Guan, X.; Wang, Z.; Zhou, Y.; Zhu, L.; Qiu, S.; Xiao, S.; Fang, Q. A Stable Luminescent Covalent Organic Framework Nanosheet for Sensitive Molecular Recognition. *CCS Chem.* **2022**, 1−27.

(13) Ascherl, L.; Evans, E. W.; Gorman, J.; Orsborne, S.; Bessinger, D.; Bein, T.; Friend, R. H.; Auras, F. Perylene-Based Covalent Organic Frameworks for Acid Vapor Sensing. *J. Am. Chem. Soc.* **2019**, *141*, 15693−15699.

(14) Cui, W.-R.; Zhang, C.-R.; Jiang, W.; Liang, R.-P.; Qiu, J.-D. Covalent Organic Framework Nanosheets for Fluorescence Sensing Via Metal Coordination. *ACS Appl. Nano Mater.* **2019**, *2*, 5342−5349.
(15) Kulkarni, R.; Noda, Y.; Kumar Barange, D.; Kochergin, Y. S.; Lyu, P.; Balcarova, B.; Nachtigall, P.; Bojdys, M. J. Real-Time Optical and Electronic Sensing with a Beta-Amino Enone Linked, Triazine-Containing 2D Covalent Organic Framework. *Nat. Commun.* **2019**, *10*, 3228.
(16) Xian, W.; Zhang, P.; Zhu, C.; Zuo, X.; Ma, S.; Sun, Q. Bionic Thermosensation Inspired Temperature Gradient Sensor Based on Covalent Organic Framework Nanofluidic Membrane with Ultrahigh Sensitivity. *CCS Chem.* **2021**, *3*, 2464−2472.
(17) Xu, J.; He, Y.; Bi, S.; Wang, M.; Yang, P.; Wu, D.; Wang, J.; Zhang, F. An Olefin-Linked Covalent Organic Framework as a Flexible Thin-Film Electrode for a High-Performance Micro-Supercapacitor. *Angew. Chem., Int. Ed.* **2019**, *58*, 12065−12069.
(18) Wu, C.; Liu, Y.; Liu, H.; Duan, C.; Pan, Q.; Zhu, J.; Hu, F.; Ma, X.; Jiu, T.; Li, Z.; Zhao, Y. Highly Conjugated Three-Dimensional Covalent Organic Frameworks Based on Spirobifluorene for Perovskite Solar Cell Enhancement. *J. Am. Chem. Soc.* **2018**, *140*, 10016−10024.
(19) Furukawa, H.; Yaghi, O. M. Storage of Hydrogen, Methane, and Carbon Dioxide in Highly Porous Covalent Organic Frameworks for Clean Energy Applications. *J. Am. Chem. Soc.* **2009**, *131*, 8875−8883.
(20) Li, M.; Liu, J.; Li, Y.; Xing, G.; Yu, X.; Peng, C.; Chen, L. Skeleton Engineering of Isostructural 2D Covalent Organic Frameworks: Orthoquinone Redox-Active Sites Enhanced Energy Storage. *CCS Chem.* **2021**, *3*, 696−706.
(21) Jin, E.; Lan, Z.; Jiang, Q.; Geng, K.; Li, G.; Wang, X.; Jiang, D. 2D Sp^2 Carbon-Conjugated Covalent Organic Frameworks for Photocatalytic Hydrogen Production from Water. *Chem* **2019**, *5*, 1632−1647.
(22) Wang, Y.; Liu, H.; Pan, Q.; Wu, C.; Hao, W.; Xu, J.; Chen, R.; Liu, J.; Li, Z.; Zhao, Y. Construction of Fully Conjugated Covalent Organic Frameworks Via Facile Linkage Conversion for Efficient Photoenzymatic Catalysis. *J. Am. Chem. Soc.* **2020**, *142*, 5958−5963.
(23) Huang, N.; Lee, K. H.; Yue, Y.; Xu, X.; Irle, S.; Jiang, Q.; Jiang, D. A Stable and Conductive Metallophthalocyanine Framework for Electrocatalytic Carbon Dioxide Reduction in Water. *Angew. Chem., Int. Ed.* **2020**, *59*, 16587−16593.
(24) Gonçalves, R. S. B.; de Oliveira, A. B. V.; Sindra, H. C.; Archanjo, B. S.; Mendoza, M. E.; Carneiro, L. S. A.; Buarque, C. D.; Esteves, P. M. Heterogeneous Catalysis by Covalent Organic Frameworks (COF): $Pd(OAc)_2$@COF-300 in Cross-Coupling Reactions. *ChemCatChem* **2016**, *8*, 743−750.
(25) Stegbauer, L.; Schwinghammer, K.; Lotsch, B. V. A Hydrazone-Based Covalent Organic Framework for Photocatalytic Hydrogen Production. *Chem. Sci.* **2014**, *5*, 2789−2793.
(26) Liu, Y.; Wu, C.; Sun, Q.; Hu, F.; Pan, Q.; Sun, J.; Jin, Y.; Li, Z.; Zhang, W.; Zhao, Y. Spirobifluorene-Based Three-Dimensional Covalent Organic Frameworks with Rigid Topological Channels as Efficient Heterogeneous Catalyst. *CCS Chem.* **2021**, *3*, 2418−2427.
(27) Lu, M.; Zhang, M.; Liu, J.; Yu, T. Y.; Chang, J. N.; Shang, L. J.; Li, S. L.; Lan, Y. Q. Confining and Highly Dispersing Single Polyoxometalate Clusters in Covalent Organic Frameworks by Covalent Linkages for CO_2 Photoreduction. *J. Am. Chem. Soc.* **2022**, *144*, 1861−1871.
(28) Yang, S.; Hu, W.; Zhang, X.; He, P.; Pattengale, B.; Liu, C.; Cendejas, M.; Hermans, I.; Zhang, X.; Zhang, J.; Huang, J. 2D Covalent Organic Frameworks as Intrinsic Photocatalysts for Visible Light-Driven CO_2 Reduction. *J. Am. Chem. Soc.* **2018**, *140*, 14614−14618.
(29) Zhao, W.; Yan, P.; Li, B.; Bahri, M.; Liu, L.; Zhou, X.; Clowes, R.; Browning, N. D.; Wu, Y.; Ward, J. W.; Cooper, A. I. Accelerated Synthesis and Discovery of Covalent Organic Framework Photocatalysts for Hydrogen Peroxide Production. *J. Am. Chem. Soc.* **2022**, *144*, 9902−9909.
(30) Gui, B.; Lin, G.; Ding, H.; Gao, C.; Mal, A.; Wang, C. Three-Dimensional Covalent Organic Frameworks: From Topology Design to Applications. *Acc. Chem. Res.* **2020**, *53*, 2225−2234.
(31) Yusran, Y.; Guan, X.; Li, H.; Fang, Q.; Qiu, S. Postsynthetic Functionalization of Covalent Organic Frameworks. *Natl. Sci. Rev.* **2020**, *7*, 170−190.
(32) Wang, S.; Da, L.; Hao, J.; Li, J.; Wang, M.; Huang, Y.; Li, Z.; Liu, Z.; Cao, D. A Fully Conjugated 3D Covalent Organic Framework Exhibiting Band-Like Transport with Ultrahigh Electron Mobility. *Angew. Chem., Int. Ed.* **2021**, *60*, 9321−9325.
(33) Uribe-Romo, F. J.; Hunt, J. R.; Furukawa, H.; Klock, C.; O'Keeffe, M.; Yaghi, O. M. A Crystalline Imine-Linked 3-D Porous Covalent Organic Framework. *J. Am. Chem. Soc.* **2009**, *131*, 4570−4571.
(34) Guan, X.; Fang, Q.; Yan, Y.; Qiu, S. Functional Regulation and Stability Engineering of Three-Dimensional Covalent Organic Frameworks. *Acc. Chem. Res.* **2022**, *55*, 1912−1927.
(35) Liang, L.; Qiu, Y.; Wang, W. D.; Han, J.; Luo, Y.; Yu, W.; Yin, G. L.; Wang, Z. P.; Zhang, L.; Ni, J.; Niu, J.; Sun, J.; Ma, T.; Wang, W. Non-Interpenetrated Single-Crystal Covalent Organic Frameworks. *Angew. Chem., Int. Ed.* **2020**, *59*, 17991−17995.
(36) Lin, G.; Ding, H.; Yuan, D.; Wang, B.; Wang, C. A Pyrene-Based, Fluorescent Three-Dimensional Covalent Organic Framework. *J. Am. Chem. Soc.* **2016**, *138*, 3302−3305.
(37) Li, H.; Ding, J.; Guan, X.; Chen, F.; Li, C.; Zhu, L.; Xue, M.; Yuan, D.; Valtchev, V.; Yan, Y.; Qiu, S.; Fang, Q. Three-Dimensional Large-Pore Covalent Organic Framework with Stp Topology. *J. Am. Chem. Soc.* **2020**, *142*, 13334−13338.
(38) Harvey, P. D. Porphyrin-Based Metal- and Covalent-Organic Frameworks as Heterogeneous Nanosized Photocatalysts in Organic Synthesis. *J. Mater. Chem. C* **2021**, *9*, 16885−16910.
(39) Kandambeth, S.; Shinde, D. B.; Panda, M. K.; Lukose, B.; Heine, T.; Banerjee, R. Enhancement of Chemical Stability and Crystallinity in Porphyrin-Containing Covalent Organic Frameworks by Intramolecular Hydrogen Bonds. *Angew. Chem., Int. Ed.* **2013**, *52*, 13052−13056.
(40) Jiao, L.; Yang, W.; Wan, G.; Zhang, R.; Zheng, X.; Zhou, H.; Yu, S. H.; Jiang, H. L. Single-Atom Electrocatalysts from Multivariate Metal-Organic Frameworks for Highly Selective Reduction of CO_2 at Low Pressures. *Angew. Chem., Int. Ed.* **2020**, *59*, 20589−20595.
(41) Zhong, H.; Wang, M.; Ghorbani-Asl, M.; Zhang, J.; Ly, K. H.; Liao, Z.; Chen, G.; Wei, Y.; Biswal, B. P.; Zschech, E.; Weidinger, I. M.; Krasheninnikov, A. V.; Dong, R.; Feng, X. Boosting the Electrocatalytic Conversion of Nitrogen to Ammonia on Metal-Phthalocyanine-Based Two-Dimensional Conjugated Covalent Organic Frameworks. *J. Am. Chem. Soc.* **2021**, *143*, 19992−20000.
(42) Han, B.; Jin, Y.; Chen, B.; Zhou, W.; Yu, B.; Wei, C.; Wang, H.; Wang, K.; Chen, Y.; Chen, B.; Jiang, J. Maximizing Electroactive Sites in a Three-Dimensional Covalent Organic Framework for Significantly Improved Carbon Dioxide Reduction Electrocatalysis. *Angew. Chem., Int. Ed.* **2022**, *134*, No. e202114244.
(43) Lv, H.; Sa, R.; Li, P.; Yuan, D.; Wang, X.; Wang, R. Metalloporphyrin-Based Covalent Organic Frameworks Composed of the Electron Donor-Acceptor Dyads for Visible-Light-Driven Selective CO_2 Reduction. *Sci. China: Chem.* **2020**, *63*, 1289−1294.
(44) Shan, Z.; Wu, M.; Zhu, D.; Wu, X.; Zhang, K.; Verduzco, R.; Zhang, G. 3D Covalent Organic Frameworks with Interpenetrated Pcb Topology Based on 8-Connected Cubic Nodes. *J. Am. Chem. Soc.* **2022**, *144*, 5728−5733.
(45) Liang, Z.; Wang, H. Y.; Zheng, H.; Zhang, W.; Cao, R. Porphyrin-Based Frameworks for Oxygen Electrocatalysis and Catalytic Reduction of Carbon Dioxide. *Chem. Soc. Rev.* **2021**, *50*, 2540−2581.
(46) Xu, X.; Cai, P.; Chen, H.; Zhou, H. C.; Huang, N. Three-Dimensional Covalent Organic Frameworks with She Topology. *J. Am. Chem. Soc.* **2022**, *144*, 18511−18517.
(47) *Materials Studio, ver. 7.0*; Accelrys Inc.: San Diego, CA, 2013.
(48) Wang, X.; Ding, X.; Wang, T.; Wang, K.; Jin, Y.; Han, Y.; Zhang, P.; Li, N.; Wang, H.; Jiang, J. Two-Dimensional Porphyrin-

https://doi.org/10.1021/jacs.2c13817
J. Am. Chem. Soc. 2023, 145, 3248−3254

Based Covalent Organic Framework with Enlarged Inter-Layer Spacing for Tunable Photocatalytic CO_2 Reduction. *ACS Appl. Mater. Interfaces* **2022**, *14*, 41122−41130.

https://doi.org/10.1021/jacs.2c13817
J. Am. Chem. Soc. 2023, 145, 3248−3254